Journal of Power Sources 195 (2010) 5619–5627

Contents lists available at ScienceDirect

Journal of Power Sources

journal homepage: www.elsevier.com/locate/jpowsour

Pre-oxidized and nitrided stainless steel alloy foil for proton exchange membrane fuel cell bipolar plates. Part 2: Single-cell fuel cell evaluation of stamped plates

Todd J. Toops[a], Michael P. Brady[a,*], Peter F. Tortorelli[a], Josh A. Pihl[a], Francisco Estevez[b], Daniel Connors[b], Fernando Garzon[c], Tommy Rockward[c], Don Gervasio[d], William Mylan[d], Sree Harsha Kosaraju[d]

[a] Oak Ridge National Laboratory, Oak Ridge, TN 37831, USA
[b] AGNI-GenCell, Southbury, CT 06488, USA
[c] Los Alamos National Laboratory, Los Alamos, NM 87545, USA
[d] Arizona State University, Tempe, AZ 85287, USA

ARTICLE INFO

Article history:
Received 14 February 2010
Received in revised form 12 March 2010
Accepted 15 March 2010
Available online 19 March 2010

Keywords:
Polymer electrolyte/proton exchange membrane (PEM) fuel cells
Nitride
Metallic bipolar plates
Durability
Corrosion resistance

ABSTRACT

Thermal (gas) nitridation of stainless steel alloys can yield low interfacial contact resistance (ICR), electrically conductive and corrosion-resistant nitride containing surface layers (Cr_2N, CrN, TiN, V_2N, VN, etc.) of interest for fuel cells, batteries, and sensors. This paper presents results of proton exchange membrane (PEM) single-cell fuel cell studies of stamped and pre-oxidized/nitrided developmental Fe–20Cr–4V weight percent (wt.%) and commercial type 2205 stainless steel alloy foils. The single-cell fuel cell behavior of the stamped and pre-oxidized/nitrided material was compared to as-stamped (no surface treatment) 904L, 2205, and Fe–20Cr–4V stainless steel alloy foils and machined graphite of similar flow field design. The best fuel cell behavior among the alloys was exhibited by the pre-oxidized/nitrided Fe–20Cr–4V, which exhibited ~5–20% better peak power output than untreated Fe–20Cr–4V, 2205, and 904L metal stampings. Durability was assessed for pre-oxidized/nitrided Fe–20Cr–4V, 904L metal, and graphite plates by 1000+ h of cyclic single-cell fuel cell testing. All three materials showed good durability with no significant degradation in cell power output. Post-test analysis indicated no metal ion contamination of the membrane electrode assemblies (MEAs) occurred with the pre-oxidized and nitrided Fe–20Cr–4V or graphite plates, and only a minor amount of contamination with the 904L plates.

1. Introduction

A key challenge for proton exchange membrane fuel cells (PEMFCs) is the development of low-cost bipolar plates amenable to rapid, high volume manufacture that can also meet stringent performance and durability requirements [1–9]. Graphite is the benchmark bipolar plate material due to its high electrical conductivity, low interfacial contact resistance (ICR), and excellent corrosion resistance in the acidic PEMFC bipolar plate environment under both oxidizing (cathode side) and reducing (anode side) conditions. However, the brittleness of graphite and the high cost of machining flow fields make graphite impractical for most commercial uses. Candidate bipolar plate materials currently under consideration include graphite/carbon-based composites, polymer-based composites with conductive graphite/carbon fillers, and coated/surface-treated metals [1–9].

Thin (~0.1 mm) stamped stainless steel alloy foils are ideal for bipolar plates from a cost and manufacturability standpoint [1–13]. However, although stainless steels exhibit low bulk electrical resistance, their ICR values are unacceptably high due to the formation of the surface oxides which confer corrosion resistance. Stainless steels can also be susceptible to metal ion dissolution in PEMFC environments, which can cause poisoning of the MEAs and loss of performance [14].

Part 1 of this paper examined the use of pre-oxidation and nitridation to form corrosion-resistant and low ICR mixed nitride-oxide surfaces on 0.1 mm thick stainless steel alloy foils in a manner amenable to commercial scale production [15]. Promising combinations of high corrosion resistance and low ICR were obtained for a developmental stainless steel alloy, Fe–20Cr–4V wt.%, and for a commercial type 2205 (Fe–22Cr–5Ni wt.% base) stainless steel alloy (Table 1), although the latter material showed some variation in ICR values due to local regions of continuous Cr-oxide formation at the surface [15]. In particular, the structure formed on the

* Corresponding author at: Oak Ridge National Laboratory, Materials Science and Technology, MS 6115, Oak Ridge, TN 37831, USA. Tel.: +1 865 574 5153; fax: +1 865 241 0215.
E-mail address: bradymp@ornl.gov (M.P. Brady).

0378-7753/$ – see front matter © 2010 Elsevier B.V. All rights reserved.
doi:10.1016/j.jpowsour.2010.03.056

Table 1
Analyzed alloy compositions (wt.%) as determined by inductively coupled plasma and combustion analysis.

Alloy name	Fe	Cr	V	Ni	Mo	Other elements
904L	Balance	22%	0.04%	24%	4.3%	1.5% Mn, 1.3% Cu, 0.33% Si, 0.09% Co, 0.06% N, 0.05% Nb, 0.05% W, 0.03% Al, 0.02% C
2205	Balance	22.1%	0.2%	5.6%	3.2%	0.49% Mn, 0.4% Si, 0.25% Cu, 0.1% Co, 0.06% W, 0.03% Nb, 0.19% N, 0.02% C
Fe–20Cr–4V	Balance	20%	3.8%	0%	0%	0.07% Mn, 0.07% Si, 0.06% N, 0.03% Ca, 0.02% C, 0.01% Al

pre-oxidized and nitrided Fe–20Cr–4V consisted of V-nitride particles dispersed throughout the thickness of the Cr-oxide [15], i.e. "through-thickness", and exhibited ICR and corrosion resistance approaching that of nitrided, high-Cr, Ni–Cr and Fe–Cr base alloys where more continuous Cr-nitride base surfaces were formed [9,16–18]. The goal of part 2 of this work was to compare the single-cell fuel cell performance of stamped and pre-oxidized/nitrided foils relative to untreated stainless steel alloy foils and benchmark graphite bipolar plates.

2. Experimental

2.1. Materials

Metallic foils of the developmental Fe–20Cr–4V and commercial type 2205 and 904L (Fe–22Cr–24Ni–4Mo wt.% base) stainless steel alloys were procured from ATI Allegheny Ludlum in ~0.1 mm thickness (analyzed compositions are shown in Table 1). The Fe–20Cr–4V and 2205 alloys were selected based on their amenability to surface modification by pre-oxidation and nitridation [15]. The 904L was selected as a benchmark material, as it is reported to exhibit excellent corrosion resistance in PEMFC environments due to its high levels of Cr, Mo, and Ni alloying additions [10]. It should be noted that 904L is among the more costly grades of austenitic stainless steel, primarily due to the high Ni and Mo content, and may be too expensive for many PEMFC applications.

To create bipolar plate flow fields, the ~0.1 mm thick stainless steel alloy foils were stamped by AGNI-GenCell Corporation to a 16 cm^2 active area single-channel, serpentine flow field design as shown in Fig. 1. The channel width averaged 1.6 mm and the channel depth averaged 0.4 mm, but due to differences in alloy ductility the depth varied by up to 0.05 mm. To provide a comparative benchmark, polished fuel cell-grade graphite plates (6.5 mm thick from ElectroChem) were machined to the same areal dimensions as the stamped metallic foils. The machined flow field channel dimensions in the graphite, graphically depicted in Fig. 2, were chosen to replicate as closely as possible the single-serpentine pathway in the stamped alloy foil. The channels in the stamped foils were more rounded at the edges and therefore an exact replication was not possible. However, the approximation is considered acceptable with respect to durability assessment and comparison of post fuel cell test metal ion contamination levels in the MEAs. It is emphasized that these flow field and plate differences between machined graphite block and thin metal stampings preclude a direct comparison in performance curves.

2.2. Surface modification

The stamped Fe–20Cr–4V and 2205 foils were treated by the pre-oxidation and nitridation process described in detail elsewhere [15]. In all cases the material was first stamped before being surface-treated. An overnight vacuum bake out at 200 °C was used to eliminate adsorbed water vapor and other oxygen-containing impurities prior to pre-oxidation and nitridation. A 15 min pre-oxidation was conducted in a flowing mixture of 4.0% H_2, 0.5% O_2, and 95.5% N_2. Nitridation was conducted for 1 h at 1000 °C in flowing 96.0% N_2 and 4.0% H_2. Heating to the pre-oxidation or nitridation reaction temperature was accomplished in 4 h, with an overnight furnace cooling. Mass gains (which reflect oxygen and nitrogen uptake into the material) for the stamped Fe–20Cr–4V and 2205 foils are shown in Table 2. All of the nitrided samples discussed in this study have undergone a pre-oxidation step, and henceforth will only be labeled as "nitrided" materials for convenience, i.e. "pre-oxidized" will be dropped from the nomenclature.

2.3. Single-cell fuel cell evaluation

Two membrane electrode assemblies (MEAs) were employed in this study—a Gore PRIMEA series 5510 and a Nafion-117-based MEA manufactured by Electrochem Incorporated. The Gore membrane was thinner (35 μm) and was employed to measure the high performance characteristics of the bipolar plate materials. It was coated with an 8 μm electrode layer with 0.4 mg Pt cm^{-2} on both the cathode and anode side. The Gore MEA was cut from the electrode area of a larger MEA, i.e. the Pt/Carbon layer covered the entire MEA in the design employed in this study. An un-integrated 380 μm gas diffusion layer (GDL), Sigracet-HM 5% from SGL, was employed with a microporous carbon layer on the MEA side. Since the catalyzed portion encompasses the entire 32 cm^2 area of this MEA, the active area is defined by the 16 cm^2 GDL. The thinness of these MEAs makes them very sensitive to imperfections or misalignment of the gaskets, and resulted in premature failure of the Gore MEAs—thus they could not be used for the long term evaluation. The thicker (180 μm) Nafion-117 membrane was employed to ensure membrane integrity for the 1000 h durability evaluation.

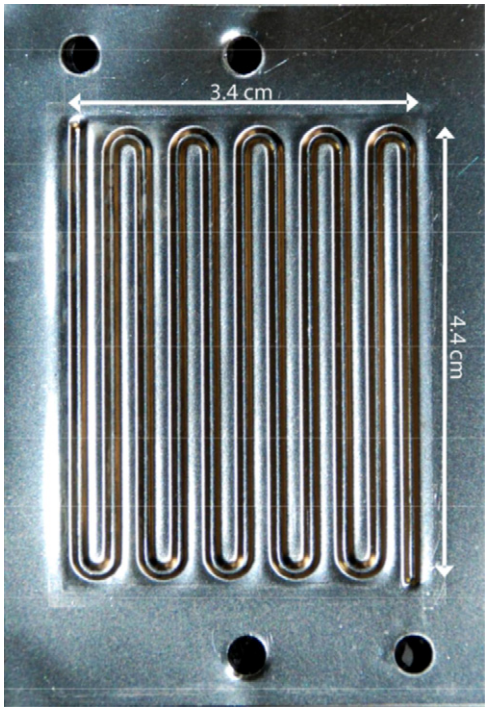

Fig. 1. Untreated stamped foil showing serpentine flow field of cathode side.

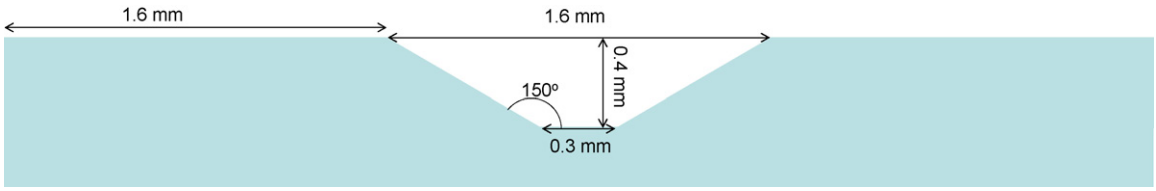

Fig. 2. Depiction of the flow channels in both the graphite plates and the alloy foils. Drawing represents cross-section of one channel and two lands.

Electrochem Inc. manufactured the Nafion-117 MEAs to match the stamped 16 cm^2 active area design. In this case, the 0.5 mg Pt cm^{-2} electrode was confined to the center of the MEA and an outer frame of the polymer was available for sealing with gaskets. Additionally, a 16 cm^2 GDL could be integrated into the MEA to ensure close contact between these two layers. The sequence for implementing these MEAs and evaluating the candidate bipolar plate materials was:

(1) Evaluate the initial performance using a Gore MEA.
(2) Evaluate the initial performance with a Nafion-117 MEA.
(3) Perform the long term durability sequence with voltage cycling and the Nafion-117 MEA.
(4) Re-evaluate the performance of the aged plates with a fresh Gore MEA.

This sequence allows the measurement of performance of the foils/plates in both the as-received and aged states.

A series of gaskets was employed to seal the fuel cell and maintain gas delivery to the serpentine flow pathway. Gasket materials were either 50–130 μm FEP (fluorinated ethylene propylene) or 250 μm Viton. The use of different MEAs also resulted in a different GDL configuration, and therefore, the gaskets used between the metal foil/graphite plate and the membrane electrode assembly (MEA) also varied. The specific gasket configurations are outlined in Fig. 3 for the anode portion of the fuel cell. The sequence is simply reversed on the cathode side and the opposite, or left-hand, serpentine pathway is employed. Since the metal foils are only 100 μm thick, the gas inlet and outlet channels could not be integrated into the foil; instead, it was necessary to rely on an inlet/outlet channel in the gasket(s) closest to the foils. This feature can be observed in gasket 2 in Fig. 3a and gaskets 2 and 3 in Fig. 3b. Additionally, the gasket in contact with the MEA does not have a channel, such that the gasket provides a level of protection for the MEA such that the flow does not impinge directly on the MEA. The configurations depicted in Fig. 3 were a result of a series of iterations and were chosen because they provided the best compromise between low external leaks, good electrical contact, and low pressure drop at the inlet of the fuel cell.

Once fully assembled, the cells were compressed using eight 6–32 bolts with application of 110 N cm of torque. Using a friction coefficient of 0.36 (based on dry threads), this corresponds to a pressure of 22 atm on the 32 cm^2 collector plates. After the initial compression, the cell was loaded into a fully automated test stand from Arbin Instruments and leak checked using an inert gas. Following the USFCC (United States Fuel Cell Council) guidelines [19], gas crossover from the anode to the cathode was investigated with a pressure differential of 0.2 atm and a total pressure of ~1.2 atm. The total system leak rate was measured to be less than 0.07 atm after 10 min, using an initial total pressure of 2.70 atm. Once these guidelines had been satisfied, 99.999% pure H_2 and compressed air were introduced to the fuel cell and the system was heated to 80 °C and pressurized to 2.73 atm on the cathode and 2.70 atm on the anode. While heating and pressurizing the fuel cell, the system was operated at a constant voltage of 0.6 V while flowing 200 cm^3 (standard temperature and pressure) per minute (sccm) of both H_2 and air. The gases were humidified to 78 °C and the gas supply lines were heated to 79 °C. The delivered % relative humidity (RH) to the 80 °C fuel cell was 94% on both the anode and cathode.

Once the fuel cell system achieved operating temperatures and pressures, the membranes were conditioned by using the following cycle: 0.6 V for 30 min, 0.4 V for 30 min, and open circuit voltage (OCV) for 1 min. This procedure was repeated for 8 cycles for the Gore MEA and 16 cycles for the Nafion-117 MEA while flowing 2.5 times the stoichiometrically required O_2 and 1.25 excess H_2; minimum cathode and anode flow rates of 100 sccm and 50 sccm, respectively, were employed when the required stoichiometric flow was low. Three successive polarization curves were then recorded by stepping down in voltage from 0.90 V to 0.40 V in 0.05 V steps that were 20 min in duration; this was then repeated in reverse as the voltage increased from 0.40 V to 0.90 V to account for hysteresis. OCV was recorded for 1 min in between polarization curves. The current was recorded for the final minute of the voltage step, and, unless otherwise noted, the third polarization curve is reported and is based on the average of the currents recorded during the increasing and decreasing voltage steps. Finally, voltage cycling was initiated for the long term durability measurements using the following cycle: 0.6 V for 30 min, 0.7 V for 20 min, 0.5 V for 20 min, and OCV for 1 min. Throughout this entire 1000+ h sequence, the fuel cell was periodically re-tightened using 110 N cm of torque.

After the plates/foils were operated in the durability tests, the MEAs were analyzed for metal ion contamination using X-ray fluorescence spectroscopy (Spectrace Quantx). Characteristic X-ray radiation was excited in the MEA samples by a rhodium tube source operated at 20 kV. The incident tube spectrum was modified by a Pd thin film energy cutoff filter to optimize the excitation and K line peak to background ratios for row 4 transition metals. A

Table 2
Nitriding procedure employed for the alloy stampings.

Alloy	Pre-oxidation		Nitridation		Bake out
	Temperature/time	Mass gain (mg cm^{-2})	Temperature/time	Mass gain (mg cm^{-2})	Temperature/time
2205					
Cathode	900 °C/15 min	0.062	1000 °C/1 h	0.184	200 °C/12 h
Anode	900 °C/15 min	0.059	1000 °C/1 h	0.201	200 °C/12 h
Fe–20Cr–4V					
Cathode	900 °C/15 min	0.042	1000 °C/1 h	0.169	200 °C/12 h
Anode	900 °C/15 min	0.043	1000 °C/1 h	0.199	200 °C/12 h

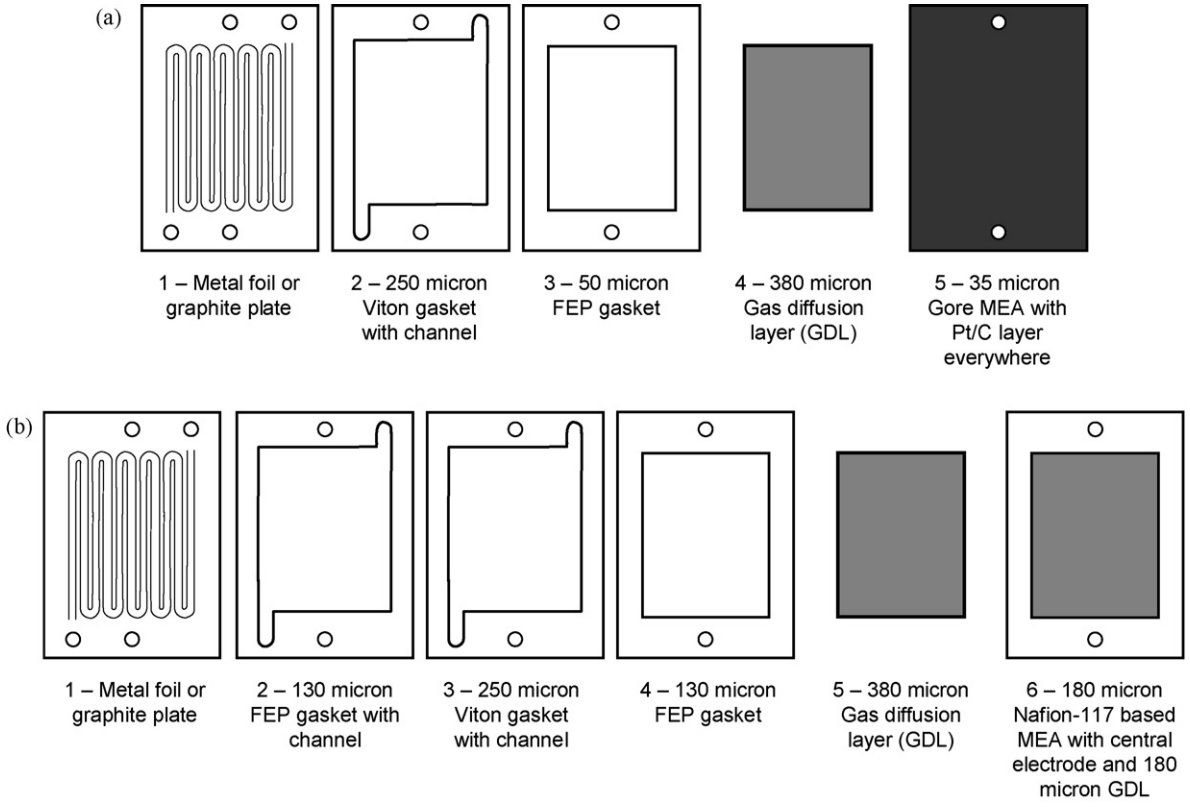

Fig. 3. Gasket sequence for anode side of the PEM fuel cell using either (a) Gore PRIMEA 5510 membrane or (b) Nafion-117 membrane.

large collimator was used to sample a 1 cm^2 area. A Fundamental Parameters Model (NIST) was used with pure element calibration samples to derive impurity concentrations from integrated K line intensities.

3. Results and discussion

Initial polarization curves were obtained with the Gore MEA for untreated 904L, Fe–20Cr–4V and 2205; nitrided Fe–20Cr–4V and 2205; and graphite (Figs. 4 and 5). The metal foils demonstrated significantly better performance than the graphite plates, and of these the nitrided Fe–20Cr–4V demonstrated the best performance (Fig. 4). The peak power obtained during these initial polarization curves is listed in the second column of Table 3 along with its associated voltage. The 30% lower peak performance for the graphite plates compared to the stamped metallic foils was attributed to differences in the machined graphite and stamped flow fields. As discussed in Section 2.1, these differences preclude direct comparison of graphite vs metal stamping performance curves in this study, and the primary use of the graphite plate is as a control for post-test analysis of the MEAs for metal ion contamination. Differences in performance of less than 5–10% are considered insignificant due to build-to-build variations, so the 4% performance difference between 904L and the nitrided Fe–20Cr–4V should be interpreted as comparable performance when employing the Gore MEA. However, the untreated Fe–20Cr–4V has 22% less peak power output compared to the nitrided Fe–20Cr–4V, so it is clear that nitriding this alloy significantly improves the performance.

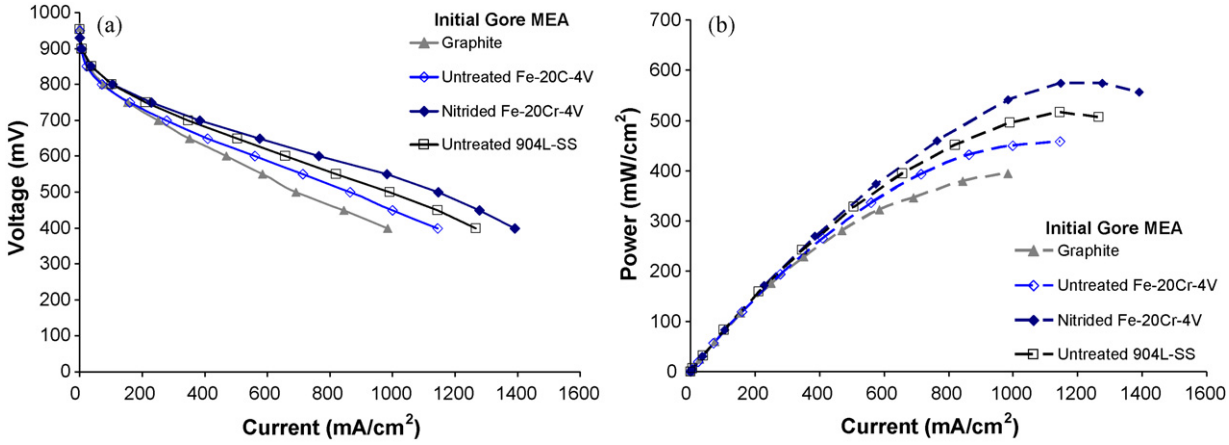

Fig. 4. Initial (a) polarization curves and (b) power output using Gore MEA with graphite, untreated Fe–20Cr–4V, nitrided Fe–20Cr–4V, and 904L. Note that the graphite performance curves cannot be compared with those of the metal stampings due to unavoidable differences in flow field and plate configuration.

Table 3
Peak power obtained during polarization curves with associated voltages in parenthesis and the corresponding ex situ ICR (1 carbon paper/flat coupon material interface) for the plates/foil materials evaluated in this study. For Gore MEAs *fresh* and *aged* refers to the state of the plate/foil only.

Plate/foil	Peak power (mW cm^{-2}) at given voltage (V)			Ex situ ICR (mΩ cm^2)
	Gore *fresh*	Gore *aged*	Nafion-117 *fresh*	
Graphite				
Untreated	402 (0.40 V)	393 (0.40 V)	186 (0.40 V)	n/a
Fe–20Cr–4V				
Untreated	458 (0.40 V)	n/a	n/a	185 [15]
Nitrided	586 (0.50 V)	546 (0.45 V)	222 (0.55 V)[a]	8 [15]
904L				
Untreated	564 (0.45 V)	538 (0.45 V)	175 (0.50 V)	125–140[b] [11]
2205				
Untreated	434 (0.45 V)	n/a	n/a	350 [15]
Nitrided	28 (0.40 V)	n/a	n/a	10–25 [15]

[a] Average of two MEAs used to age the single foil.
[b] Measured on a plate of 904L rather than a foil.

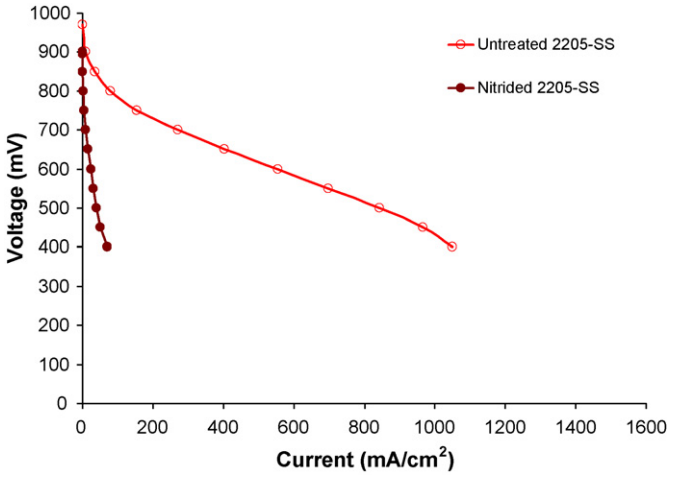

Fig. 5. Polarization curves using Gore MEA with untreated and nitrided 2205.

In contrast to the Fe–20Cr–4V results, the nitrided 2205 exhibited a peak power decrease of 94% compared to untreated 2205 (Fig. 5 and Table 3). The poor performance of the nitrided 2205 was attributed to formation of continuous regions of insulating Cr_2O_3 in the surface-treated zone (further microstructural details are presented elsewhere [15]). It is interesting to note that although ex situ coupon studies of nitrided 2205 showed variation in ICR values suggestive of possible local regions of continuous oxide, the values were still significantly lower than untreated 2205 [15]. It is speculated that the scatter in pre-oxidation/nitridation surface chemistry formed on small 2205 stainless steel foil coupons (typically ~20 mm × 10 mm range) may have become exacerbated with the larger surface area of the stamped plates (greater chance for local thick regions of Cr_2O_3). It is also possible that preferential conductance on the nitride surface over the coupon edges, rather than true through-thickness conductance, may have contributed to artificially low ICR values for surface-treated 2205. Caution should therefore be exercised in relying solely on ex situ ICR measurements for assessment of surface-treated alloys. The poor behavior of the 2205 also highlights the importance of the V addition in Fe–20Cr–4V for forming through-thickness V_xN particles, which provide a conductivity path through the Cr_2O_3 that forms during pre-oxidation. This structure is partially due to the stronger nitride-forming tendency of V compared to Cr and also because the oxides and nitrides of V and Cr are mutually soluble [18].

While the above results are promising with respect to the pre-oxidation and nitridation treatment of the Fe–20Cr–4V alloy, long term durability and assessment of possible degradation in performance due to metal ion dissolution or contact resistance increase are major concerns. Therefore, the nitrided Fe–20Cr–4V was selected for a 1000 h voltage cycling evaluation using a Nafion-117 MEA. Untreated 904L and graphite plates were also subjected to the same test conditions in order to benchmark performance.

The initial polarization and power curves of these plate materials with Nafion-117 are shown in Fig. 6 with the peak power output listed in Table 3. Although there is lower power output compared

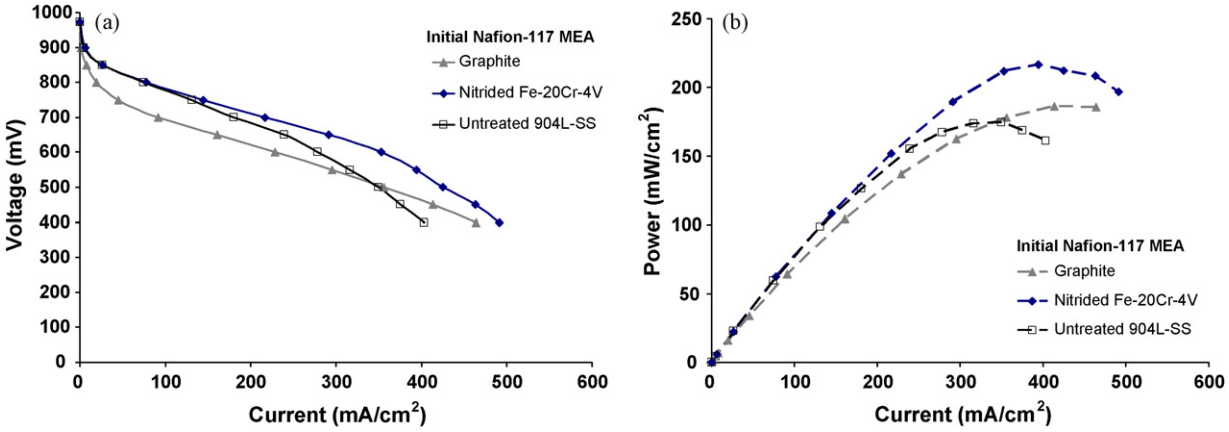

Fig. 6. Initial (a) polarization curves and (b) power output using Nafion-117 MEA with graphite, nitrided Fe–20Cr–4V, and 904L. Note that the graphite performance curves cannot be compared with those of the metal stampings due to unavoidable differences in flow field and plate configuration.

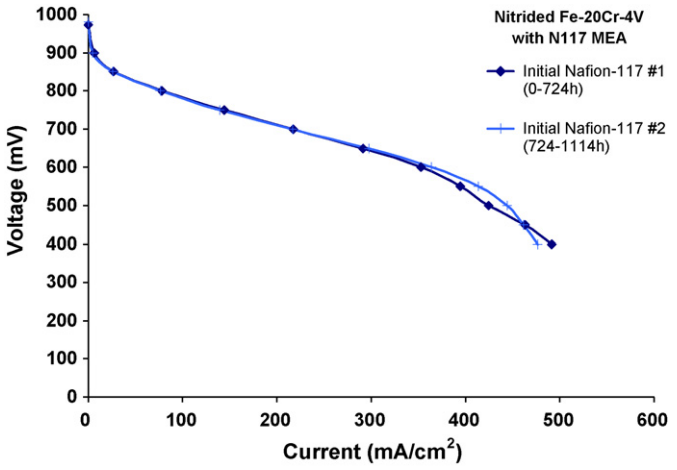

Fig. 7. Initial polarization curves for the two Nafion-117 MEAs used for the durability evaluation of the nitrided Fe–20Cr–4V metal foils.

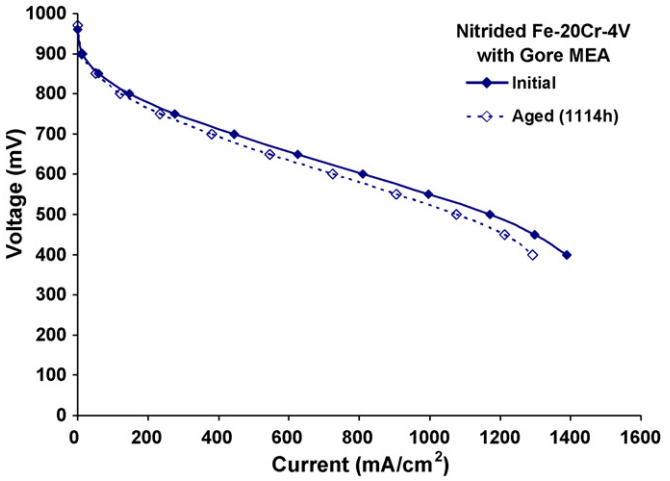

Fig. 9. Comparison of the initial and final aged polarization curves obtained for nitrided Fe–20Cr–4V using the Gore MEA.

to the Gore MEA (the Nafion-117 was 5× thicker than the Gore and employed a different GDL), similar trends were observed for each material. The one exception to the trends occurred at higher current densities where the power production of the treated Fe–20Cr–4V and untreated 904L foils decrease relative to the graphite plates (Fig. 6b vs Fig. 4b). In particular, the performance of the 904L decreases to the point that it drops below that of the graphite plate at voltages less than 0.5 V; in fact, the peak power for 904L is 6% less than graphite.

The cause of this decrease relative to the results for the Gore MEA is unclear, but the following factors are expected to contribute. The first is that the Gore MEA does not have an integrated GDL. The initial contact between the MEA and GDL is made during the fuel cell build, and since the GDL is not hot-pressed into the thin MEA there is likely a significant contact resistance between these two materials. Therefore, at high power outputs in the Gore MEA configuration, the overriding contact resistance is between the GDL and MEA which results in similar curves for both metals and the graphite in the Gore case. When employing the Nafion-117 MEA, the initial GDL has been incorporated into the MEA and therefore, should have low contact resistance. Under this scenario, the GDL/plate interface would have a more significant role in the overall performance than in the Gore MEA scenario. As reported in Table 3 and in detail elsewhere [15], nitrided Fe–20Cr–4V exhibits an ICR value (single carbon paper/material interface) of 8 mΩ cm^2 at 150 N cm^{-2} as compared to a reported value for 904L of 150 mΩ cm^2 [11]. This lower ICR is speculated to contribute to the moderately better performance for the nitrided Fe–20Cr–4V over that of untreated 904L.

Continuous operation for over 1000 h was achieved for each of the materials using the specified voltage cycle (0.6 V for 30 min, 0.7 V for 20 min, 0.5 V for 20 min and OCV for 1 min). There were no scheduled shutdowns and start-ups, but each material incurred at least one power outage that resulted in a forced restart. Unfortunately, the MEA being used in the nitrided Fe–20Cr–4V had to be replaced after 724 h of voltage cycling, and therefore two MEAs were used. The second MEA ran from 724 h to 1114 h of total operation for the nitrided Fe–20Cr–4V test plates. As shown in Fig. 7, the initial polarization curves for both Nafion-117 MEAs used for the nitrided Fe–20Cr–4V durability evaluation were very similar. In comparing the initial polarization curve to the aged polarization curves, the average of the two polarization curves shown in Fig. 7 was used. Fig. 8 details the progression of the cell performance during durability testing using both of the Nafion-117 MEAs. The averaged current density and OCV for each cycle is presented for the entire nitrided Fe–20Cr–4V durability evaluation. The re is some cycle-to-cycle variation in the data, but there is not a significant decrease in performance over the lifetime of the evaluation.

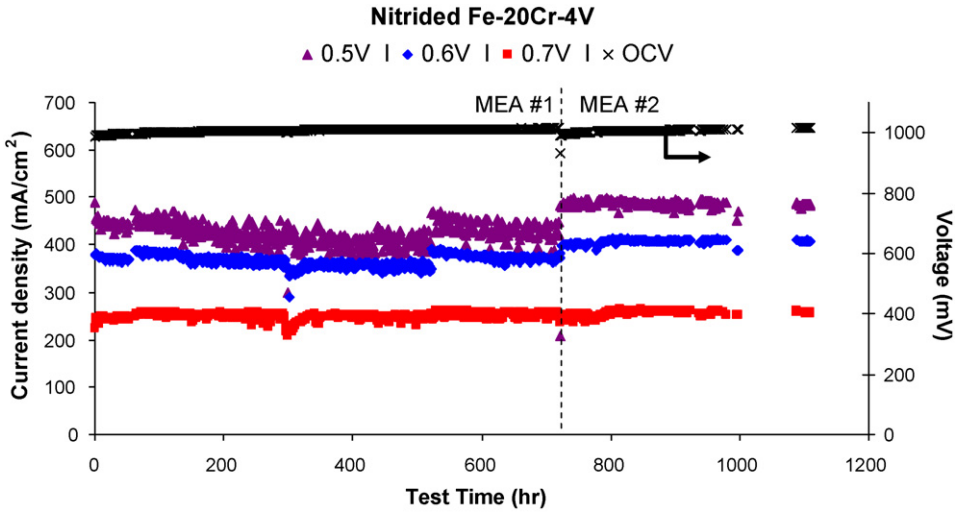

Fig. 8. The averaged current density and OCV for each cycle for the entire nitrided Fe–20Cr–4V durability evaluation with the Nafion-117 MEA.

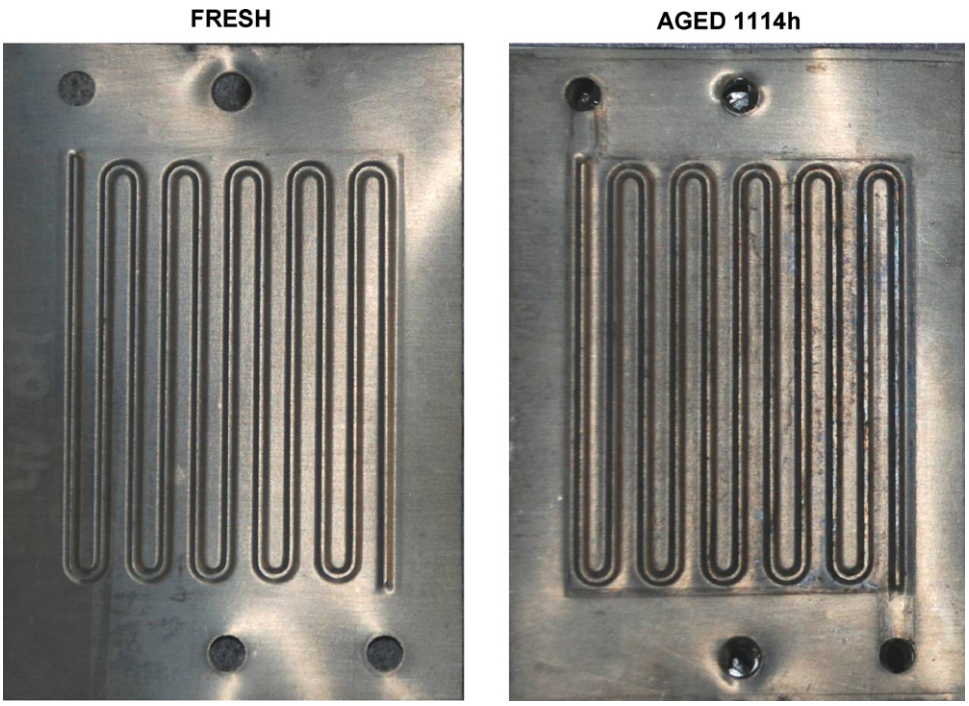

Fig. 10. Photographs of the nitrided Fe–20Cr–4V in the fresh state and after voltage cycling for 1114 h.

The discontinuities in the data noted after 300 h and 500 h stemmed from restarting the test stand following a power outage; additionally, there was a loss of data after 1000 h. Fig. 9 compares the performance of the aged nitrided Fe–20Cr–4V test plates obtained with the Gore MEA to the initial performance obtained with the plates prior to durability testing. The peak power outputs were similar (Table 3) and polarization curves showed little evidence for degradation of the plates. There was a slight decrease in performance after the durability test with 7% less power output; however, this is within the range of the expected build-to-build variability. Combining these Gore MEA results (Fig. 9) with the Nafion-117 MEA results (Fig. 8), it can be concluded that the nitrided Fe–20Cr–4V foil performance was essentially unaffected by voltage cycling over 1114 h of operation. This supposition was consistent with visual inspection of the test plates before and after durability testing (Fig. 10).

The same approach outlined for the nitrided Fe–20Cr–4V foil was employed on the graphite plate and the untreated 904L foil. The durability evaluation results for the graphite plates (Fig. 11) reveal cycle-to-cycle variability similar to that seen for the Fe–20Cr–4V plates with no observable performance degradation. As in the nitrided plate durability evaluation, issues associated with power failures or loss of back pressure can be noted in Fig. 11; one such restart resulted in a notable drop in performance after 800 h. The polarization curves for the fresh and aged graphite plates with the Gore MEA (Fig. 12) are nearly identical, and the drop in peak power for the aged plate is less than 2% (Table 3), suggesting that there was no detrimental impact from voltage cycling on the graphite plate. The 904L foil also exhibited similar behavior with respect to cycle-to-cycle variability and overall durability (Fig. 13). The Gore MEA comparison, shown in Fig. 14, confirms that voltage cycling for over 1000 h results in only a minor loss of performance at the

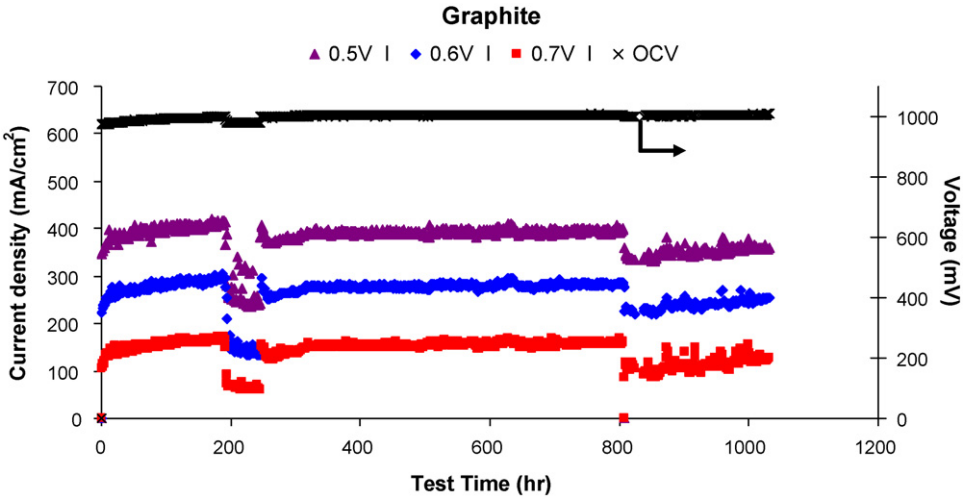

Fig. 11. The averaged current density and OCV for each cycle for the entire graphite plate durability evaluation using the Nafion-117 MEA.

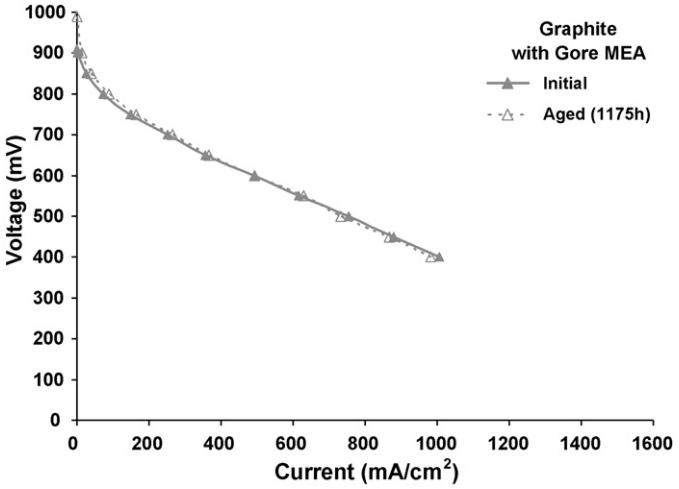

Fig. 12. Comparison of the initial and final aged polarization curves obtained for graphite using the Gore MEA.

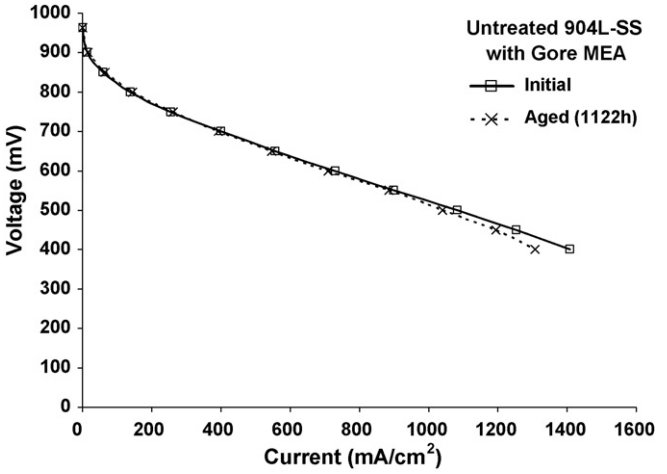

Fig. 14. Comparison of the initial and final aged polarization curves obtained for 904L using the Gore MEA.

highest current densities, with less than 5% difference between the initial and aged peak power outputs (Table 3).

After durability testing, the MEAs used with all three plate materials were analyzed for metal ion contamination by XRF (Table 4). The metal contamination levels for both MEAs used in the nitrided Fe–20Cr–4V test plates were at the background MEA level, similar to that obtained with the graphite test plates and comparable to the levels present in fresh MEAs. This finding is consistent with the excellent performance durability for the nitrided Fe–20Cr–4V over the course of the 1114 h of voltage cycling (Fig. 9) and further indicates that the MEA failure at 724 h was not due to metal contamination (note that the Fe contamination values were actually lower after testing with graphite and nitrided plates than the levels measured in the fresh MEAs, this is a result of leaching of the Fe from the MEAs during the course of fuel cell operation). The MEA from the 904L test plates showed minor levels of metal contamination, 1.1 $\mu g\,cm^{-2}$ Fe and 0.18 $\mu g\,cm^{-2}$ Cr (Table 4), consistent with the excellent reported corrosion resistance of this alloy in PEMFC environments [10] and significantly less than the ~10–100 $\mu g\,cm^{-2}$ levels of metal contamination generally reported when using less corrosion-resistant grades such as type 316 stainless steel [12–14]. The levels observed with the 904L were still, however, ~3–5× higher than the 0.1–0.2 $\mu g\,cm^{-2}$ Fe and <0.05 $\mu g\,cm^{-2}$ Cr detected

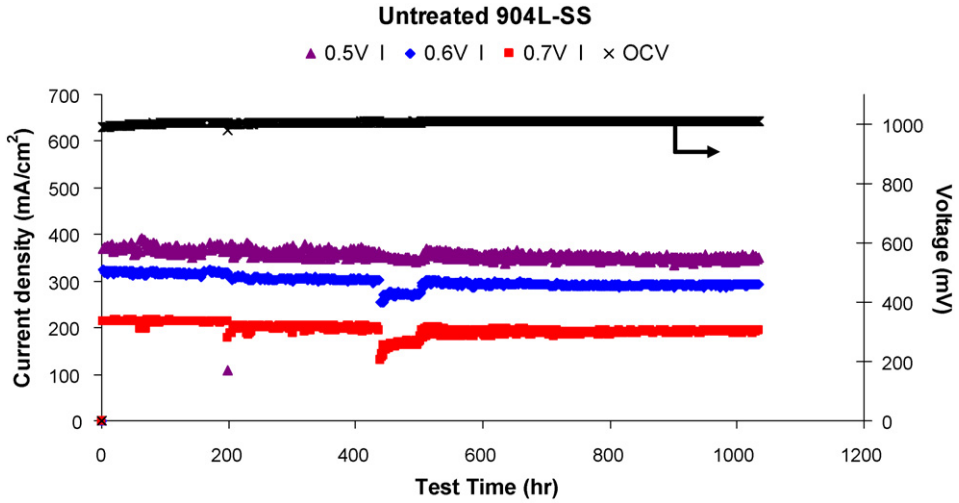

Fig. 13. The averaged current density and OCV for each cycle for the entire untreated 904L durability evaluation using the Nafion-117 MEA.

Table 4
Quantitative results of X-ray fluorescence (XRF) spectroscopy* of the Nafion-117 MEAs used in the durability evaluations.

Foil/plate used	Fe ($\mu g\,cm^{-2}$)	Cr ($\mu g\,cm^{-2}$)	V ($\mu g\,cm^{-2}$)	Ni ($\mu g\,cm^{-2}$)
N/A (fresh MEA)	0.5	<0.05	<0.05	<0.05
Nitrided Fe–20Cr–4V				
0–724 h	0.1	<0.05	<0.05	<0.05
724–1114 h	0.2	<0.05	<0.05	<0.05
Graphite	0.1–0.3	<0.05	<0.05	<0.05
Untreated 904L	1.1	0.18	<0.05	0.11

* Detection limits ~0.05 $\mu g\,cm^{-2}$.

in the MEAs used with the nitrided Fe–20Cr–4V and graphite plates.

4. Summary and conclusions

The nitrided Fe–20Cr–4V (untreated) 904L, and graphite plates all exhibited good durability in the cyclic single-cell fuel cell evaluations conducted in the present work. Although the 904L performed well with respect to corrosion durability and MEA contamination, its high ICR values are expected to be a significant drawback when used in fuel cell stacks, where contact resistance aspects will be more important than the highly torqued single-cell testing of the present work (a torque of 110 N cm was used in the present work, which corresponds to a compaction force of >200 N cm^{-2}. This level exceeds the DOE ICR goal (derived from stack targets) of ~150 N cm^{-2} loading, but was needed in the present work to achieve a reasonable (low) level of system leak rate). The results of the present work suggest that stamped and pre-oxidized/nitrided Fe–20Cr–4V foils show good potential for use as PEMFC bipolar plates due to their combination of low ICR and high corrosion resistance. Consistent single-cell performance was maintained over the course of 1114 h of total operation using a cycle of open circuit voltage for 1 min, 0.60 V for 30 min, 0.70 V for 20 min, and 0.50 V. Post-test analysis of the MEAs indicated that the pre-oxidation and nitridation surface treatment successfully prevented metal contamination. Future work will focus on evaluation of the amenability of the Fe–20Cr–4V alloy to stamping of complex, state-of-the-art flow field designs, assessment of the repeatability and robustness of the pre-oxidation and nitridation treatment under conditions representative of mass production, and further optimization of the pre-oxidation and nitridation treatment with regards to lower reaction temperatures and shorter cycle times to further decrease cost.

Acknowledgements

The authors thank William P. Partridge and Burak Ozpineci for reviewing this manuscript. The authors also thank G.W. Garner for performing the pre-oxidation nitridation exposures, and J.M. Rakowski of ATI Allegheny Ludlum for the Fe–20Cr–4V, 2205, and 904L foils. Funding from the U.S. Department of Energy's Hydrogen, Fuel Cells, and Infrastructure Program is gratefully acknowledged. ORNL is managed by UT-Battelle, LLC for the US DOE under contract DE-AC05-00OR22725. *Notice*: This submission was sponsored by a contractor of the United States Government under contract DE-AC05-00OR22725 with the United States Department of Energy. The United States Government retains, and the publisher, by accepting this submission for publication, acknowledges that the United States Government retains, a nonexclusive, paid-up, irrevocable, worldwide license to publish or reproduce the published form of this submission, or allow others to do so, for United States Government purposes.

References

[1] V. Mehta, J.S. Cooper, J. Power Sources 114 (1) (2003) 32–53.
[2] A. Hermann, T. Chaudhuri, P. Spagnol, Int. J. Hydrogen Energy 30 (12) (2005) 1297–1302.
[3] H. Tawfik, Y. Hung, D. Mahajan, J. Power Sources 163 (2) (2007) 755–767.
[4] E. Middelman, W. Kout, B. Vogelaar, J. Lenssen, E. de Waal, J. Power Sources 118 (1–2) (2003) 44–46.
[5] Y.Y. Shao, G.P. Yin, Z.B. Wang, Y.Z. Gao, J. Power Sources 167 (2) (2007) 235–242.
[6] N.D.L. Heras, E.P.L. Roberts, R. Langton, D.R. Hodgson, Energy Environ. Sci. 2 (2) (2009) 206–214.
[7] J.F. Wu, X.Z. Yuan, J.J. Martin, H.J. Wang, J.J. Zhang, J. Shen, S.H. Wu, W. Merida, J. Power Sources 184 (1) (2008) 104–119.
[8] X.Z. Yuan, H.J. Wang, J.J. Zhang, D.P. Wilkinson, J. New Mater. Electrochem. Syst. 8 (4) (2005) 257–267.
[9] M.P. Brady, B. Yang, H. Wang, J.A. Turner, K.L. More, M. Wilson, F. Garzon, JOM (Journal of Metals, Minerals, and Materials Society) 58 (August (8)) (2006) 50–57.
[10] D.P. Davies, P.L. Adcock, M. Turpin, S.J. Rowen, J. Power Sources 86 (1–2) (2000) 237–242.
[11] H.L. Wang, M.A. Sweikart, J.A. Turner, J. Power Sources 115 (2) (2003) 243–251.
[12] J. Wind, R. Spah, W. Kaiser, G. Bohm, J. Power Sources 105 (2) (2002) 256–260.
[13] R.C. Makkus, A.H.H. Janssen, F.A. de Bruijn, R.K.A.M. Mallant, J. Power Sources 86 (1–2) (2000) 274–282.
[14] A. Pozio, R.F. Silva, M. De Francesco, L. Giorgi, Electrochim. Acta 48 (11) (2003) 1543–1549.
[15] M.P. Brady, H. Wang, J.A. Turner, H.M. Meyer III, K.L. More, P.F. Tortorelli, B.D. McCarthy, J. Power Sources 195 (2010) 5619–5627.
[16] M.P. Brady, K. Weisbrod, I. Paulauskas, R.A. Buchanan, K.L. More, H. Wang, M. Wilson, F. Garzon, L.R. Walker, Scripta Mater. 50 (7) (2004) 1017–1022.
[17] M.P. Brady, H. Wang, B. Yang, J.A. Turner, M. Bordignon, R. Molins, M. Abd Elhamid, L. Lipp, L.R. Walker, Int. J. Hydrogen Energy 32 (16) (2007) 3778–3788.
[18] B. Yang, M.P. Brady, H. Wang, J.A. Turner, K.L. More, D.J. Young, P.F. Tortorelli, E.A. Payzant, L.R. Walker, J. Power Sources 174 (1) (2007) 228–236.
[19] Single Cell Test Protocol, United States Fuel Cell Council, Document #05-014B.2, July 2006.